



- 1 Effects of the Three Gorges Dam Operation on the
- 2 hydrological interaction between the Yangtze River and
- 3 downstream aquifers
- $5 \quad Qi \; Zhu^1, \; Ye \; Kang^1, \; Zhang \; Wen^{1*}, \; Hui \; Liu^1, \; Luguang \; Liu^2, \; Yan \; Li^2, \; Xu \; Li^3, \; Eungyu$
- 6 Park⁴

7

- 8 1. ¹Hubei Key Laboratory of Yangtze Catchment Environmental Aquatic Science,
- 9 School of Environmental Studies, China University of Geosciences, Wuhan 430074,
- 10 Hubei, People's Republic of China
- 11 2. Hubei Water Resources Research Institute, Wuhan 430070, People's Republic of
- 12 China
- 13 3. School of Earth and Environment, Anhui University of Science and Technology,
- 14 Huainan, People's Republic of China
- 15 4. Department of Geology, Kyungpook National University, Daegu, Republic of
- 16 Korea

1718

19 Correspondence to: Zhang Wen (wenz@cug.edu.cn)





Abstract. The construction of the Three Gorges Dam (TGD) has profoundly altered 20 the groundwater cycle downstream. The obscure spatiotemporal patterns of exchange 21 fluxes between the Yangtze River and groundwater hinder the resolution of water 22 resources and environmental issues in the watershed. In the Four-Lake Basin, the first 23 river-lake wetland plain downstream of the TGD, this study investigated the spatial 24 extent of the Yangtze River's influence on adjacent groundwater by leveraging 25 multiple groups of monitoring wells installed along the river. A coupled SWAT-26 MODFLOW model was applied to quantify period-specific SW-GW exchanges. A 27 counterfactual scenario without TGD operation-holding other conditions constant is 28 also simulated for comparison. The results show: (1) The influence range of the 29 Yangtze River on confined groundwater is larger in the ZJ-JLX2 section, whereas it is 30 relatively minor on groundwater near HH1 profile and HH2 profile. The influence 31 distance at the HH1 profile is the smallest, measuring as 1.94 km. (2) River and 32 33 groundwater exchanges exhibit pronounced seasonal and spatial characteristics: riverto-aquifer recharge dominates during drawdown and flooding periods, while aquifer-34 35 to-river discharge dominates during impounding and dry periods. Using JLX2 as a divider, interaction rates are consistently higher in the upper section than in the lower 36 one. (3) Relative to natural conditions, TGD operation dramatically dampens Yangtze 37 River-groundwater interactions overall. The effect is most pronounced during the dry 38 period in the upper section, when the interaction rate decreases by 40.6%. These 39 research outcomes serve as a vital theoretical foundation for assessing the effects of 40 the Three Gorges Dam's regulation on the regional water cycle. 41





42 1 Introduction

43 High-dam reservoirs play a critical role in flood mitigation, hydroelectric power generation, water supply, and navigation (Poff et al., 1999). To date, approximately 44 50% of rivers worldwide are regulated by dams (Van Cappellen et al., 2016). The 45 dam's impact on the riparian hydrology and biogeochemistry is so pronounced 46 (Palmer and Ruhi, 2019; Song et al., 2020; Maavara et al., 2020) that it can even 47 surpass the effects of hydrological extremes (Dewey et al., 2022). The Three Gorges 48 Dam (TGD), a mega-engineering structure on the mainstream of the Yangtze River, 49 functioned as a "master valve" controlling flow in the middle reaches. Operational 50 strategies such as "storing water in early autumn" and "releasing water in winter and 51 spring" have substantially altered the river's natural hydrological regime (Wang et al., 52 2016; Guo et al., 2022). 53 54 Centrally located in the Middle Yangtze Basin, the Four-Lake Basin is the first large river-lake wetland system downstream of the TGD. It supports an integrated 55 ecosystem of rivers, lakes, reservoirs, and farmlands (Zhang et al., 2023) and plays a 56 vital role in flood regulation, ecological stabilization, and sustaining agricultural 57 economies (Zhou et al., 2013). However, since the TGD became operational, nitrogen and phosphorus pollution in the water bodies of the middle Yangtze River basin, 59 particularly in areas such as the Four-Lake Basin, has intensified (Gao et al., 2021; Hu 60 et al., 2023; Zhou et al., 2023). While extensive research has documented the impacts 61 62 of the TGD on the regional water cycle (e.g., Deng et al., 2016; Xiong et al., 2020; Wu et al., 2023), the precise quantification of these effects remains a critical and 63 64 ongoing challenge in the field. Unlike surface-water-dominated systems, many lakes, rivers, and agricultural 65 wetlands in the Four-Lake Basin interact with the Yangtze mainly through subsurface 66 groundwater exchange (Deng et al., 2016). Yet the extent of the Yangtze's influence, 67





which is a key driver of regional hydrological and ecological processes (Hu et al., 68 2023; Lai et al., 2025), remains poorly quantified, hindering a clear understanding of 69 groundwater cycling and its ecological consequences. Moreover, TGD operations 70 have introduced significant spatiotemporal variations in water levels along the 71 Yangtze mainstream. Combined with the high spatial heterogeneity of 72 hydrogeological conditions in the riparian zone, these changes complicate efforts to 73 characterize river-groundwater interactions. Although prior research has illuminated 74 local-scale exchange processes (Wang & Wörman, 2019; Huang et al., 2023), such 75 insights are insufficient for assessing basin-wide impacts, underscoring the need for 76 broader monitoring and systematic investigation. 77 Since the TGD's completion, its effects on various downstream ecological 78 components, such as lake levels (Huang et al., 2021), wetland evolution (Zhang et al., 79 2012), sediment transport (Yang et al., 2007), channel morphology (Sun et al., 2012; 80 Yang et al., 2014), and eco-hydrological conditions affecting vegetation (Xie et al., 81 2014), have attracted considerable research attention. Nevertheless, the dam's impacts 82 83 on groundwater systems remains inadequately understood, especially in terms of quantitative attribution isolated from other influencing factors. In the Four-Lake Basin, 84 the presence of an intricate flood-control network further complicates the study of 85 water interactions (World Bank, 2023). 86 87 While previous quantitative studies have examined hyporheic exchange in the Jianghan Plain (Du et al., 2018; Jiang et al., 2022), they do not fully account for the 88 compounded effects of climate, TGD operations, spatial heterogeneity in 89 hydrogeological conditions, and local flood-control and irrigation infrastructure on 90 Yangtze-groundwater interactions in the Four-Lake Basin. To be more precise, in 91 addition to being influenced by the Yangtze River, groundwater levels along the river 92 are often affected by factors such as runoff generation and concentration, surface soil 93





111

make traditional groundwater numerical modeling approaches struggle to accurately 95 capture fluctuations in the groundwater table, thereby introducing significant errors in 96 97 characterizing the exchange processes between the Yangtze River and groundwater. Despite this complexity, coupled modeling frameworks such as SWAT-MODFLOW 98 99 have been successfully employed in similar contexts to investigate regional surface water-groundwater (SW-GW) interactions (Aliyari et al., 2019; Yang et al., 2024). 100 101 Thus, developing a tailored SW-GW coupled model for simulating Yangtzegroundwater dynamics in the Four-Lake Basin is both necessary and feasible. 102 103 Aiming to bridge these gaps, this study focuses on the interplay between the 104 Yangtze River and groundwater in the Four-Lake Basin. Data from seven monitoring profiles will be used to demarcate the spatial influence of the river on aquifer 105 dynamics. The core of our approach is to develop a field-calibrated SWAT-106 MODFLOW model to analyze the effects of TGD operations on SW-GW interactions. 107 Ultimately, by constructing a counterfactual scenario without the dam, we aim to 108 109 isolate and quantify the specific impact of the TGD, providing a quantitative assessment of its influence. 110

water infiltration, and recharge from the local surface water network. These factors

2 Overview of the Study Area

Situated downstream of the TGD on the middle Yangtze's northern bank, the Four-Lake Basin covers an area of about 11,547 km² (Fig. 1). Its boundaries are formed by a combination of natural and artificial features: the northwestern hills of Jingmen and Jiangling Counties and the Zhang River irrigation district to the northwest, the Han River Basin watershed to the north, and the Yangtze River itself to the east and south. The basin's climate is characterized by a mean annual temperature



123

124

125

126

127



of 15~17 °C, with annual precipitation and evaporation averaging 1,269 mm and 1,200 mm, respectively. Precipitation is concentrated in the warm months from April to August, whereas the most intense evaporation occurs from April to October.

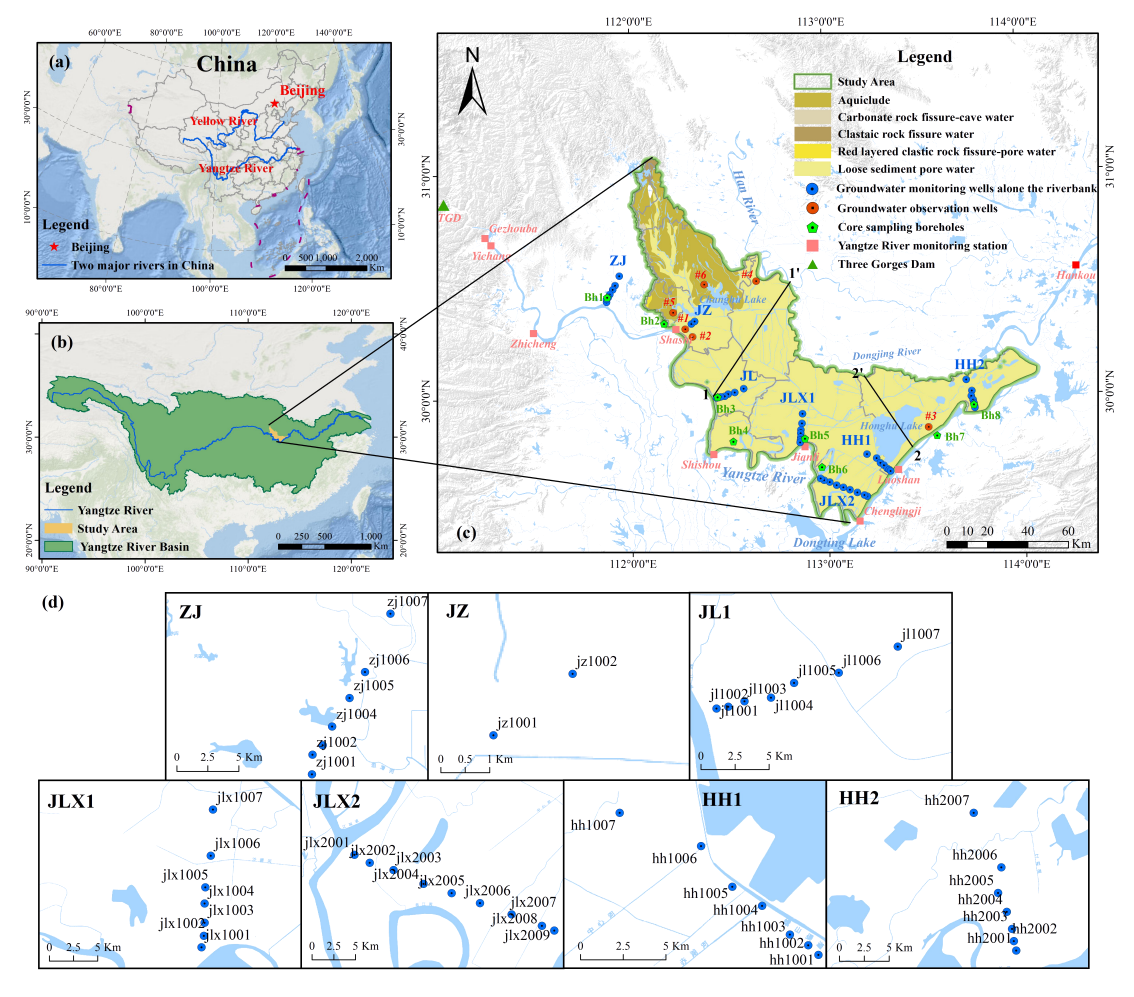


Figure 1: Map of the study area and monitoring network in the Four-Lake Basin, showing (a) the regional context of the Yangtze River (adapted from the basemap in Esri., 2023), (b) the basin location (adapted from the basemap in Esri., 2023), (c) surface water and groundwater monitoring stations in the map indicating different types of groundwate, which is entirely compiled according to the internal survey data from the author's institution, and (d) groundwater monitoring wells installed along each profile.



129

130

131

132

133

134

135

136

137

138

139

140

141

142

143

144

145

146

147

148

149

150



The Four-Lake Basin features predominantly flat topography, with an average elevation of 27 m. The area features a dense network of interconnected lakes, rivers, and canals, among which Honghu and Changhu Lakes are the most prominent. The Four-Lake Main Channel, as the primary artery of the basin, connects these major lakes and their tributaries, ultimately discharging into the Yangtze River. The study area features a groundwater system composed of an unconfined aquifer and multiple confined aquifers. The unconfined aquifer, primarily distributed across the flat central and eastern basin, consists of silty clay, silt, and fine sand, with localized thin gravel layers. Its thickness typically ranges from 3 to 10 m. The confined aquifer system includes two distinct layers. The upper confined aguifer, which is the most extensive in the region, is composed of clay, silty clay, muddy silty clay, sand, and gravel. Its thickness exhibits considerable spatial variation, generally increasing from the western and peripheral zones toward the central and eastern parts of the basin. In contrast, the lower confined aquifer is predominantly composed of gravel (Huang et al., 2023). Groundwater in the study area is primarily recharged by precipitation and exhibits strong interactions with surface water systems in some localities. Its dynamics are predominantly governed by seasonal rainfalland surface water fluctuations. The water table is generally shallow, typically lying 2~5 m below the surface, which facilitates widespread groundwater utilization. The dominant land uses, comprising aquaculture ponds, farmland, urban areas, lakes, and rivers, collectively position the basin as a key hub for agricultural and aquaculture production in China (Wang et al., 2022).





3 Data and Methods

3.1 Data Sources

We established a network of groundwater monitoring profiles along the northern bank of the Yangtze River within the Four-Lake Basin, comprising seven distinct profiles-Zhijiang (ZJ), Jingzhou (JZ), Jiangling (JL), Jianli1 (JLX1), Jianli2 (JLX2), Honghu1 (HH1), and Honghu2 (HH2)-with a total of 46 monitoring wells (Fig. 1). Within each profile, wells were systematically positioned at distances of 1, 2, 3, 5, 7, 10, 15, 20, and 25 km from the landside toe of the Yangtze River embankment. Groundwater levels were monitored from January 1 to December 31, 2021, at regular 5-day intervals.

The SWAT model primarily required two types of data: spatial data (including elevation, land use, and soil type data) and meteorological data, with the specific data formats and sources listed in Table 1. The MODFLOW model necessitated hydrogeological parameters, recharge and discharge components, and calibration data derived from long-term groundwater level observations.

Table 1 Data types and sources of SWAT model.

| Data Type | Data Accuracy | Description | Sources |
|-------------------------------|------------------|---|---|
| Digital Elevation Model (DEM) | 30 m×30 m | ASTERG DEM V3 | Geospatial Data Cloud Platform https://www.gscloud.cn/ |
| Landuse Data | 1km×1km | Distribution of land use types | Data Center for Resources and Environmental Sciences https://www.resdc.cn/ |
| Soil Type Data | 30m×30 m | Soil type and soil physical properties | Harmonized World Soil Database https://www.fao.org/ |
| Meteorological Data | 1/8°×1/8° | Daily average relative humidity, daily cumulative 24-hour precipitation, daily average solar radiation, daily maximum and minimum temperatures, and daily | China Meteorological Assimilation Driving Datasets (CMADS V1.2) https://poles.tpdc.ac.cn/ |





average wind speed

The calibration of the MODFLOW model utilized groundwater level data (2011-2013) obtained from a hydrogeological field investigation conducted in the Jianghan Plain during this period (Wen et al., 2017), nearly a decade after the impoundment of the TGD. To maintain consistency, the same timeframe was adopted for the surface hydrological modeling data in SWAT to facilitate the model's validation.

3.2 Research Methods

3.2.1 Analysis of water-level spatial response

Given that the unconfined aquifer along the Yangtze River is subject to multiple factors—including river stage, precipitation, surface water bodies, and human activities—the water level exhibits frequent fluctuations. This study, therefore, focuses on quantifying the lateral influence of the river on the more stable confined aquifer along its north bank. To this end, water-level data from the confined aquifer were collected through monitoring profiles to investigate the fluctuation patterns of both the river stage and the confined groundwater, as well as the spatial extent of the river's influence. The analytical procedure is detailed below:

(1) Data collection and analysis. The river stages and corresponding groundwater levels from the seven monitoring profiles (ZJ, JJ, JL, JLX1, JLX2, HH1, and HH2) with complete 2021 datasets were selected for analysis (Fig. 1). For each month, the daily maximum water level of the Yangtze River was identified, and the corresponding groundwater levels in monitoring wells at various distances were recorded simultaneously. The differences between the maximum water levels of the Yangtze River and groundwater in consecutive months were calculated to derive the fluctuation amplitudes of both at a monthly interval. As shown in the subplot of the ZJ profile in Fig. A1 in the Appendix A, the legend "1/9–2/17" indicates that January





9 and February 17 represent the days when the peak water levels of the Yangtze River occurred in their respective months. The difference in water levels between these two days forms the black polyline in the figure. It is important to note that the monthly maximum water level of the Yangtze River was selected because the peak value is the most prominent and objectively identifiable feature, avoiding subjectivity in selecting dates during periods of mild fluctuation. Moreover, the high water level exerts the strongest driving force on the adjacent groundwater, theoretically maximizing the reflection of groundwater response to changes in the Yangtze River water level.

(2) Construction and fitting of water-level spatial response equations. A critical step in this analysis was to develop empirical equations that quantify the response of groundwater levels to fluctuations in the Yangtze River stage at different distances from the river. Unlike previous studies, such as Wang and Wörman (2019), which focused mainly on temporal variations in groundwater, the present study employs the analytical solution proposed by Liu et al. (2021) to demonstrate the exponential attenuation of groundwater response amplitudes with distance from the riverbank under sinusoidal river-stage variations, which can be expressed as:

$$207 \quad y = a \cdot e^{bx} \tag{1}$$

where y represents the variation amplitude of the groundwater level [m]; x represents the distance from the monitoring point to the riverbank [m]; a represents the change of the Yangtze River water level within a specific period [m]; b represents the attenuation coefficient [1/m]. For each monitoring profile shown in Fig. A1, eleven polylines derived from the monthly water level differences are generated. Then those polylines exhibiting abnormal patterns due to measurement errors or localized hydrological influences are excluded. For each remaining polyline, Eq. (1) is applied for fitting to inversely estimate the corresponding a and b values. The multiple b





- values from each cross-section are then averaged to obtain \overline{b} , which is a new section-
- 217 specific attenuation coefficient for Eq. (1).
- 218 (3) Delineation of lateral influence extent. In hydrogeological practice, the
- 219 intensity of river influence on lateral groundwater dynamics is commonly
- 220 characterized by a dimensionless parameter K, defined as the ratio of the groundwater
- 221 level fluctuation amplitude to the simultaneous river stage fluctuation amplitude.
- Therefore, by reformulating Equ. (1) and substituting the value of \bar{b} obtained from
- 223 Step (2), the formula for calculating the K value for each monitoring cross-section can
- 224 be expressed as

$$225 \quad K = y/a = e^{\bar{b}x} \tag{2}$$

- According to established criteria (He and Cai, 1999), when K < 0.02, i.e., when
- 227 the groundwater fluctuation falls below 2% of the corresponding river stage
- 228 fluctuation, the river is considered to have no significant influence on the groundwater.
- Thus, the distance from the riverbank corresponding to K = 0.02 was taken as the
- 230 maximum lateral influence extent of the Yangtze River on the confined aquifer.
- Therefore, with the value of \overline{b} obtained in Step (2), the value of x, which indicates the
- 232 lateral influence range of the Yangtze River on groundwater, can be determined
- 233 inversely by assigning a value to K.
- 234 3.2.2 SWAT-MODFLOW coupling model for the Four-Lake Basin
- The SWAT model for the Four-Lake Basin was developed in ArcSWAT, with all
- 236 data sources detailed in Table 1. The modeling framework began with watershed
- 237 delineation, dividing the basin into 35 subbasins based on Digital Elevation Model
- 238 (DEM) data and the river network. Hydrologic Response Units (HRUs) were
- 239 generated by overlaying land use classification, soil types, and slope categories,





ultimately producing 428 HRUs as illustrated in Fig. 2. Meteorological data was extracted from the CAMADS v1.2 dataset at 288 monitoring stations within and around the basin (Fig. 2f). The simulation spanned a three-year warm-up period (2008-2010), followed by calibration (2011-2014) and validation (2015-2016) phases, all performed at a monthly temporal resolution.

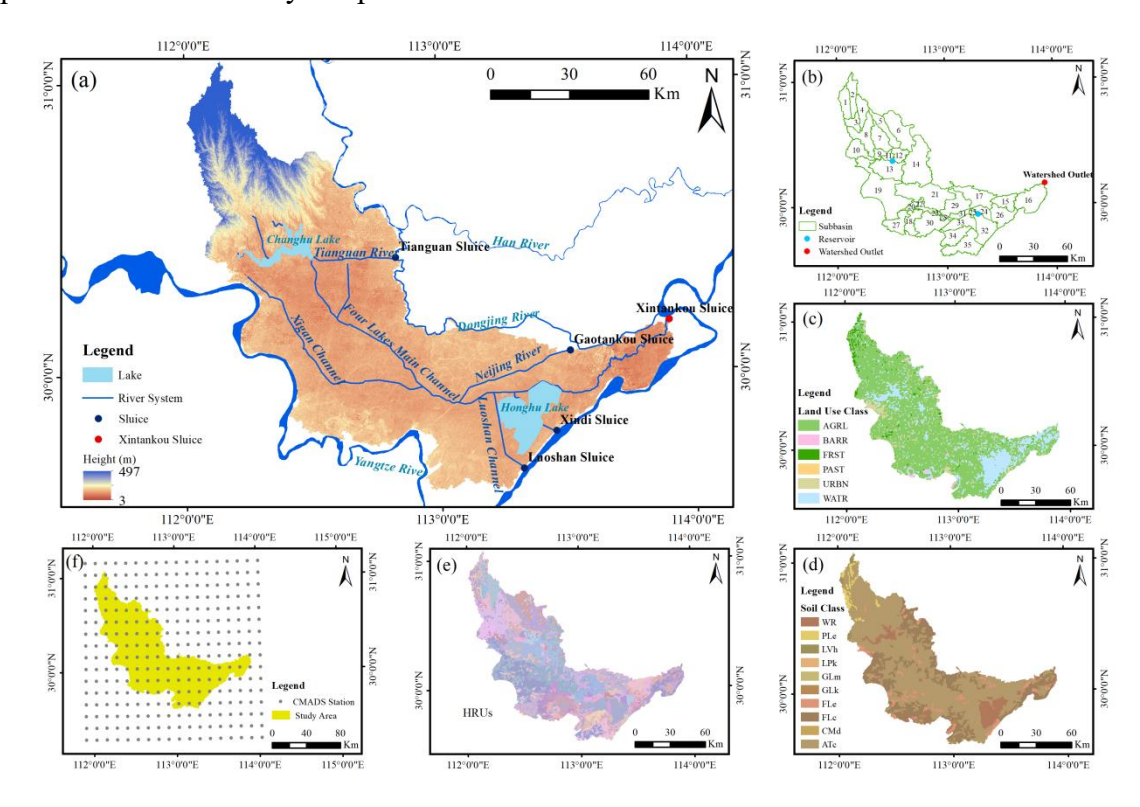


Figure 2: (a) Four-Lake Basin elevations, major water systems, and major sluices. (b) SWAT Model subbasins and watershed outlets. (c) Land use classification. (d) Soil cclassification. (e) SWAT Model HRUs. (f) CMADS V1.2 stations.

A groundwater numerical simulation using the finite difference method was performed with Visual MODFLOW Flex 9.0. Based on regional hydrogeological conditions and borehole lithological data, a heterogeneous, anisotropic, and transient groundwater flow model for the Four-Lake Basin was generalized into three layers:





253 an unconfined aquifer, an aquitard, and a confined aquifer. The model was discretized horizontally into 1 km × 1 km grids and vertically into three layers based on 254 255 hydrogeological stratification, resulting in 33,450 active cells. Hydrogeological 256 parameter zones, values, and boundary conditions are detailed in Fig. A2 and Table 257 A1 in the Appendix A. 258 The SWAT-MODFLOW coupled model was developed by establishing a one-toone correspondence between SWAT Hydrologic Response Units (HRUs) and 259 260 MODFLOW grid cells. The calibrated SWAT model provided monthly groundwater 261 recharge (GW RCHG) and actual evapotranspiration data, which were then assigned to the corresponding MODFLOW cells. These outputs were directly used as inputs for 262 263 the Recharge (RCH) and Evapotranspiration (EVT) packages in MODFLOW, thereby 264 driving the groundwater flow simulation.

4 Result and Discussion

265

266

4.1 The influence range of the Yangtze River on lateral groundwater

267 The response of confined groundwater levels to fluctuations in the Yangtze River 268 stage was evaluated across seven monitoring profiles (ZJ, JZ, JL, JLX1, JLX2, HH1, and HH2) at increasing distances (x) from the river. As illustrated in Fig. A1, the 269 270 sensitivity of groundwater levels to river stage diminishes with distance. One notable 271 deviation is observed along the ZJ profile, where anomalously large groundwater 272 fluctuations occur 5~10 km from the riverbank, possibly due to local hydrogeological 273 heterogeneity or anthropogenic influences. The amplitude-distance relationships for both the Yangtze River and groundwater levels, fitted using Equation (1) across all 274 275 seven monitoring profiles, are shown in Fig. A3 in the Appendix A. For clarity, results from a representative period of the year are displayed. All fitted curves 276



281

282

283

284

285

286

287

288



277 demonstrate a high goodness-of-fit ($R^2 > 0.9$), indicating highly reliable correlations.

278 Based on these relationships, the range of estimated b values and the corresponding

279 fitting equations for each profile were calculated, as summarized in Table 2.

Table 2 The range of estimated values of b and corresponding fitting equations for each profile

| Section | The range of estimated values of b | Attenuation fitting equation |
|---------|------------------------------------|---------------------------------|
| ZJ | -0.1271~-0.4081 | $K_{zj} = e^{-0.3064}x$ |
| JZ | -0.3375~-0.3569 | $K_{zj} = e^{-0.3463}x$ |
| JL | -0.3272~-0.4432 | $K_{\rm jl} = e^{-0.3687}x$ |
| JLX1 | -0.556~-0.8021 | $K_{\rm jlx1} = e^{-0.6935}x$ |
| JLX2 | -0.2546~-0.5289 | $K_{\rm jlx2} = e^{-0.3824}x$ |
| HH1 | -1.7839~-2.5305 | $K_{\rm hh1} = e^{-2.0203}x$ |
| HH2 | -1.4486~-2.0477 | $K_{\text{hh}2} = e^{-1.7638}x$ |

To quantify the intensity and maximum lateral extent of the Yangtze River's influence on the adjacent confined aquifer, the criterion defined in step (3) was applied. According to this criterion, the distance x corresponding to a relative groundwater fluctuation (K) of 0.02 represents the maximum influence distance. Table 3 presents the calculated maximum influence distances and the mean attenuation coefficients (b) for each monitoring profile. At the same time, Fig. 3 visually depicts the influence distances across a range of K values, including this maximum extent.

Table 3 Distance x from the riverbank corresponding to K = 0.02 and average attenuation coefficient \bar{b} for each profile.

| Profiles | ZJ | JZ | JL | JLX1 | JLX2 | HH1 | HH2 |
|----------|---------|---------|---------|---------|---------|---------|---------|
| X | 12.77 | 11.30 | 10.61 | 5.64 | 10.23 | 1.94 | 2.22 |
| <i>b</i> | -0.3064 | -0.3463 | -0.3687 | -0.6935 | -0.3824 | -2.0203 | -1.7638 |



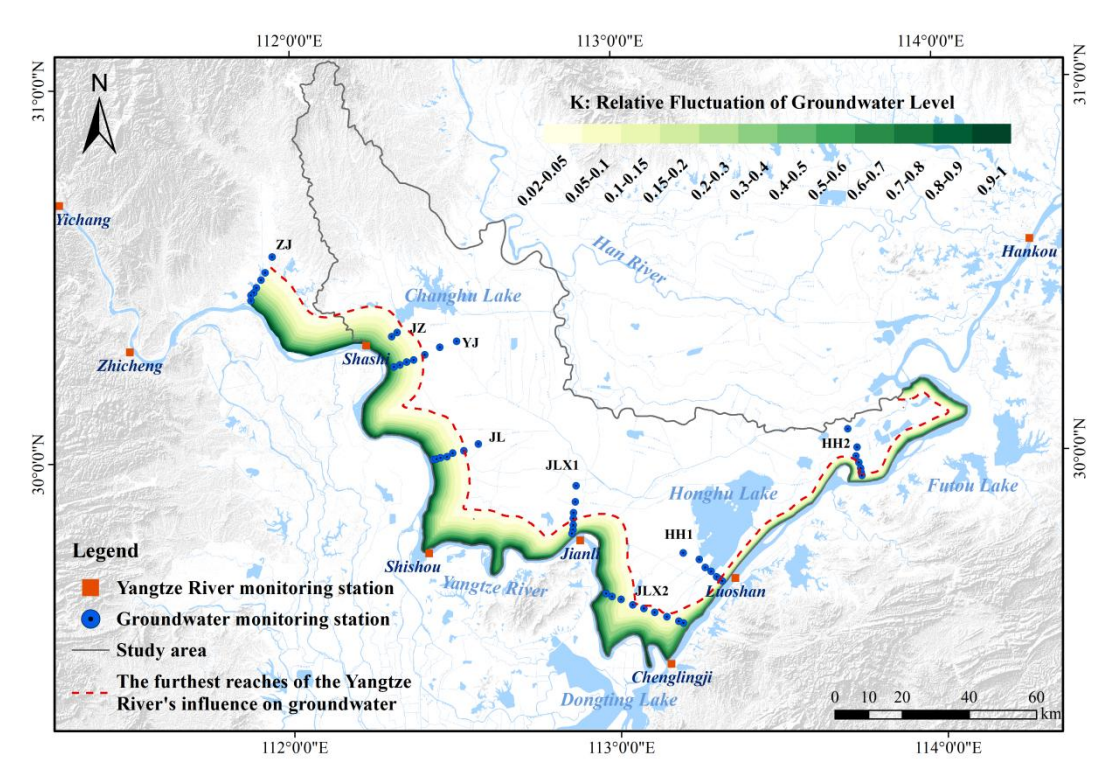


Figure 3: Different degrees and ranges of influence of the Yangtze River on the lateral confined groundwater in the Four-Lake Basin.

As summarized in Table 3 and Fig. 3, the influence of the Yangtze River on confined groundwater in the Four-Lake Basin displays clear spatial zonation, divided by the JLX2 profile into two distinct segments: ZJ-JLX2 and JLX2-HH2. The ZJ-JLX2 segment exhibits a substantially wider influence range compared to the JLX2-HH2 segment, characterized by three key features:

(1) Extended influence range: The ZJ-JLX2 segment shows a smaller attenuation coefficient (\overline{b}) and a maximum influence distance of 12.77 km (Table 3), indicating more efficient pressure transmission through the aquifer system than in the downstream segment.





304

305

306

307

308

309

310

311

312

313

314

315

316

317

318

319

320

321

322

323

324

325

groundwater systems.

(2) Hydraulic head differences primarily drive groundwater response. Due to its proximity to the TGD, the ZJ-JLX2 segment experiences amplified river-stage fluctuations that propagate over long distances. In contrast, the JLX2-HH2 segment lies downstream of the Yangtze after regulation by Dongting Lake, where river stage variations are markedly dampened, leading to a shorter propagation distance of hydraulic signals. (3) Favorable hydrogeological conditions: The JL profile, representative of the ZJ-JLX2 segment, consists of highly permeable gravel-cobble formations (Fig. A4a), which minimize hydraulic head loss and support long-distance transmission of riverinduced fluctuations. Although the 2021 Yangtze River Sediment Bulletin indicates that the river incises into the confined aquifer in the JLX2-HH2 segment, Fig. A4b shows that near the HH1-HH2 area, the aquifer materials are dominated by fine sands. The resulting lower permeability and higher flow resistance cause rapid attenuation of head fluctuations, thus restricting the lateral extent of the river's influence. Furthermore, the proximity of Honghu Lake to the HH1-HH2 segment warrants consideration. Although not in direct hydraulic contact with the confined aquifer, this extensive shallow lake interacts dynamically with the overlying phreatic aquifer. As shown in Fig. A4(b), the shallow aguitard in the vicinity of Honghu Lake exhibits significant spatiotemporal heterogeneity in thickness, facilitating localized hydraulic connectivity between the unconfined and confined aquifer systems. Under these conditions, Honghu Lake acts as a hydrological buffer; that is, its relatively stable water levels attenuate the transmission of Yangtze River stage fluctuations to adjacent





4.2 Validation of the SWAT-MODFLOW model

The SWAT model for the Four-Lake Basin was calibrated and evaluated using SWAT-CUP. A total of 17 key parameters were selected for sensitivity analysis and calibration, with 1,000 iterations conducted to optimize model performance. Table A2 summarizes the calibrated parameters, their fitted values, and sensitivity ranks. Monthly surface runoff data from the Xintankou station (outlet of sub-basin 16) from 2011 to 2016 were used for both model calibration (2011-2014) and validation (2015-2016). As shown in Fig. 4, the model performed well, achieving Nash-Sutcliffe efficiency (NSE) values of 0.7 and 0.65 during calibration and validation, respectively, and R² values of 0.76 (calibration) and 0.67 (validation), indicating satisfactory agreement between simulated and observed runoff.

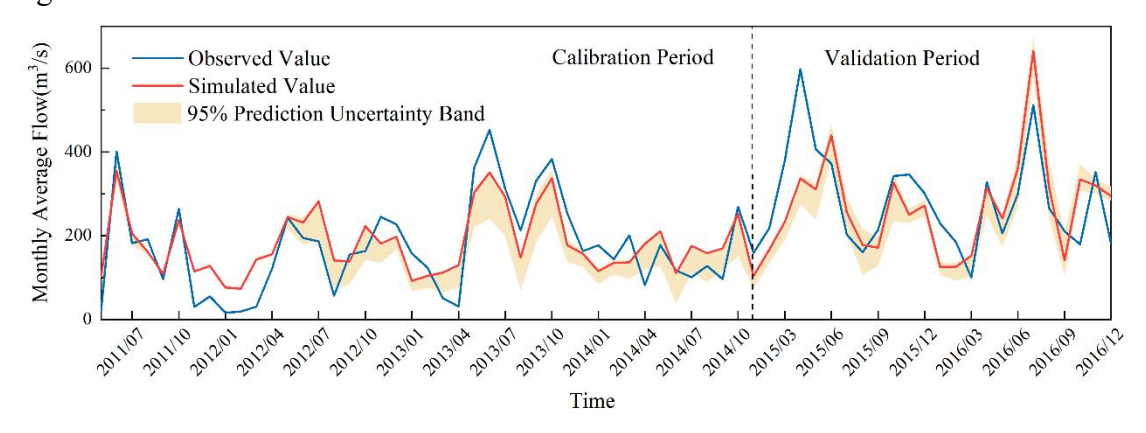


Figure 4: The fitting between the simulated monthly flow that has been calibrated and the observed one.

The coupled SWAT-MODFLOW model was calibrated against observed groundwater levels from six monitoring wells from 2011 to 2013 distributed near Yangtze River (Fig. 1). As shown in Fig. 5, the simulated groundwater levels agree well with the observed values throughout the simulation period, demonstrating the capability of the model to reproduce regional groundwater dynamics. These results





confirm that the integrated model reliably captures the key characteristics of surface water-groundwater interactions in the Four-Lake Basin.

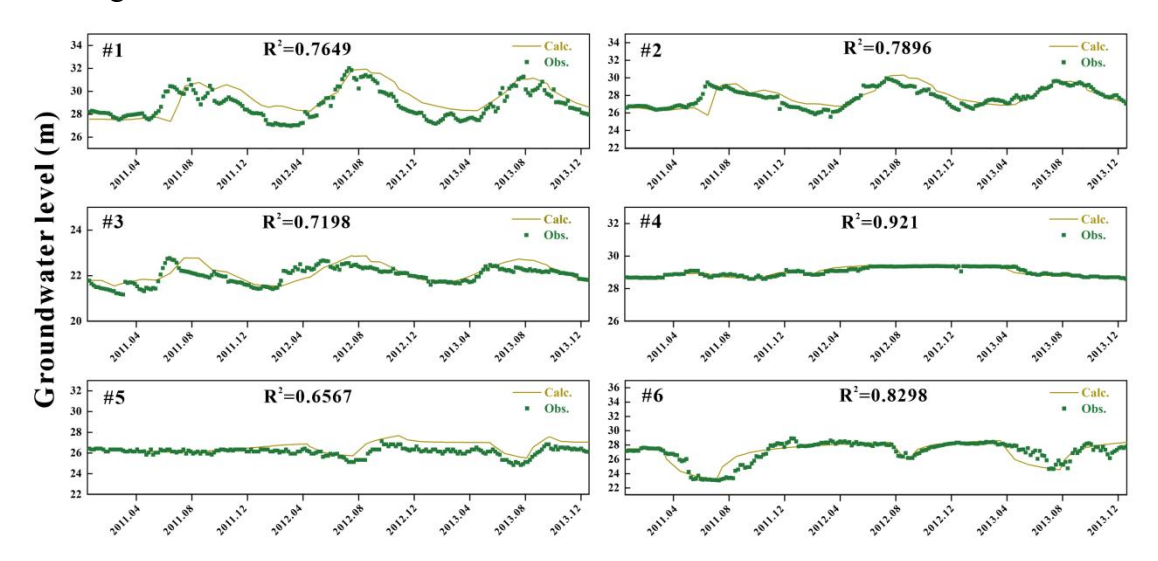


Figure 5: Fitting between the Observed groundwater levels and the calculated ones at the monitoring wells during the simulated period.

4.3 Yangtze River-groundwater interaction under TGD regulation: Spatiotemporal patterns

Figure 6 illustrates the daily exchange volume between the Yangtze River and groundwater in the mainstream within the Four-Lake Basin, calculated by the SWAT-MODFLOW model at 15-km intervals. The relative magnitudes are represented by bar charts, with blue and red indicating groundwater recharge from and discharge to the Yangtze River, respectively. The four subplots correspond to the four scheduling periods of the TGD: (1) Drawdown period. This period refers to the pre-flood water release phase, during which the water level of the TGD is lowered below the flood limit level through controlled discharge to prepare for flood peak retention and attenuation; (2) Flooding period. This period represents the subsequent flood season, during which the reservoir intercepts floods and adjusts the timing of downstream





flood peaks; (3) Impounding period. This period denotes the post-flood water storage phase, where water at the end of the flood season is stored for use during dry periods; (4) Dry period. This period is set for the water stored in the previous period to release to supplement downstream flow during dry seasons. The results in the figure represent the daily average exchange rate over all days within each operational period.

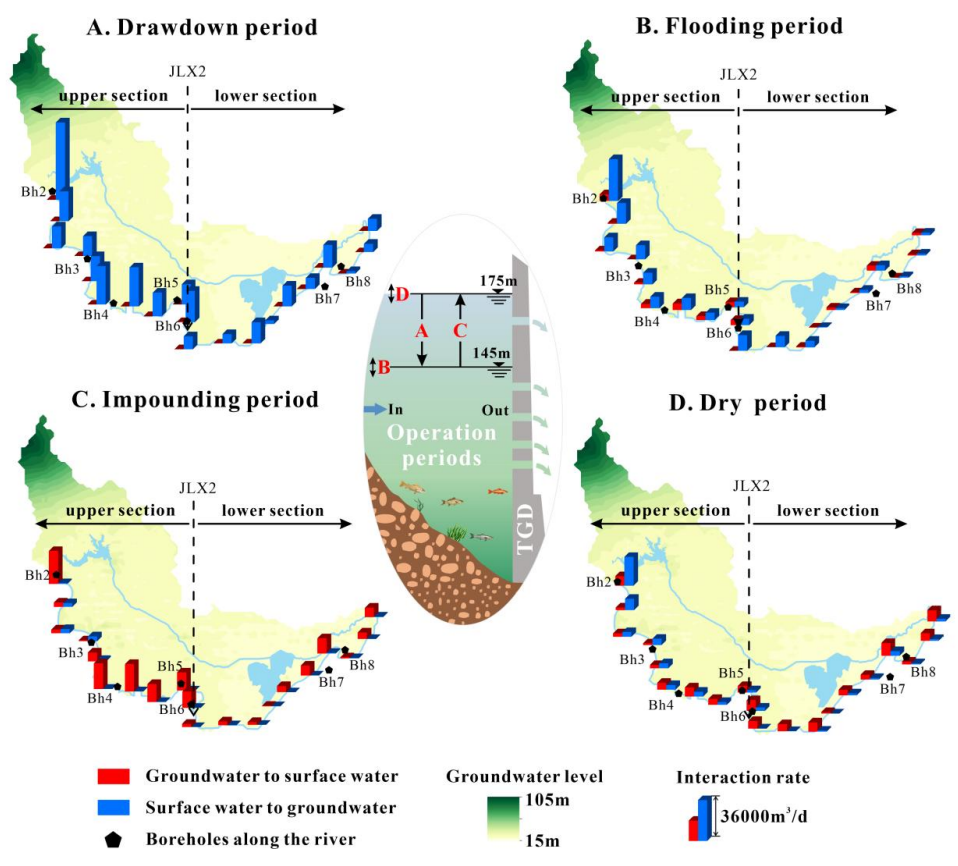


Figure 6: Spatial variations in interaction rates (average of 2011 and 2013, m³/d) between the Yangtze River and groundwater in the Four-Lake Basin during the four operational periods of the TGD. Red histograms denote groundwater discharge to surface water; blue histograms denote surface-water recharge to groundwater. TGD operational periods: A-Drawdown period, B-Flooding period, C-Impounding period and D-Dry period.

As shown in Fig. 6, river-to-aquifer recharge dominates during both the drawdown period and the flooding period, while aquifer-to-river discharge prevails in





the other two periods. Moreover, the recharge rate during the drawdown period is significantly higher than that during the flooding period. It occurs because during the drawdown period, the TGD gradually lowers the reservoir level from 175 m at the end of the previous winter to below 145 m (referenced to the Yellow Sea Datum) and releases the incoming spring flows upstream. The substantial outflow leads to a marked rise in the downstream river stage, amplifying the hydraulic gradient between the river and adjacent groundwater and driving strong river-to-aquifer recharge. During the flooding period, groundwater levels are considerably elevated due to rainfall infiltration and surface water recharge in the Four-Lake basin, which have been confirmed by our SWAT-MODFLOW simulation. Additionally, TGD operations during this period aim to attenuate downstream flood peaks for safety, thereby significantly reducing the hydraulic gradient between the river and groundwater compared to that during the drawdown period. It explains why the apparent river-groundwater exchange is weaker during the hydrologically more dynamic flooding period, as observed in Fig. 6.

During the impounding period and the dry period, the aquifer-to-river discharge intensity is higher in the former than in the latter. This difference arises because during the impounding period, groundwater levels remain elevated following the end of the flood season, while the TGD begins to impound upstream water in preparation for the dry-season water supply. This process enlarges the hydraulic gradient between groundwater and the Yangtze River. In contrast, during the dry period, groundwater levels have declined, and the TGD releases water to supplement downstream flow, which reduces the hydraulic gradient between groundwater and the river. It explains why the aquifer-to-river discharge intensity is stronger during the impounding period than during the dry period.



400

401

402

403

404

405

406

407

408

409

410

411

412

413

414

415

416 417

418

419

420

421

422

423



In addition, dividing the Yangtze River at the JLX2 monitoring section into an "upper section" and a "lower section" (as shown in Fig. 6) reveals consistently higher exchange rates in the upper one. This pattern arises because the upper section is closer to and more influenced by TGD regulation than the lower section, leading to larger stage fluctuations and weaker along-stream attenuation, which together enhance the hydraulic gradient. In contrast, the lower section, characterized by a wider channel and greater hydraulic connectivity with tributaries, exhibit a comparatively weaker response to the Three Gorges Dam operations. As shown in Fig. A5 in the Appendix A, wavelet coherence analysis reveals that with increasing distance from the TGD, the downstream river stage exhibits a progressive damping in its response to reservoir release variations, accompanied by a lengthening phase lag. Moreover, the along-river lithology profile in Fig. A6 reveals a distinct shift in aquifer composition: the upstream banks are dominated by highly permeable gravel and coarse sand, which sharply contrasts with the less permeable fine sand that constitutes the downstream deposits. The strong heterogeneity of the riparian stratigraphy is also a significant factor contributing to the weaker downstream interactive strength compared to that upstream.

4.4 Yangtze River-groundwater interaction with and without TGD: A counterfactual comparison

Against the backdrop of numerous factors influencing Yangtze River-groundwater interactions, this study isolated the effect of TGD regulation by implementing simulated "no-TGD" river stages from Wang et al. (2013) in the SWAT-MODFLOW mode. All other input data, such as precipitation, evaporation, groundwater levels, and tributary/lake stages, remained unchanged. This setup produced the results of river leakage to groundwater and groundwater discharge to





river shown in Figures 7(a) and 7(b), respectively: they illustrate the monthly variations in daily exchange rates between the Yangtze River and groundwater for the upper section, lower section, and the entire mainstream of the Four-Lake basin, demarcated by the JLX2 monitoring section. Here, the daily interaction rate represents the monthly total interaction amount averaged over all the days in that month, visualized using bar charts: red bars indicate aquifer-to-river discharge, and blue bars represent river-to-aquifer recharge. The green line graph in Figs. 7(a) amd 7(b) depict the net daily exchange, calculated as river leakage minus groundwater discharge. Fig. 7(a) shows simulation results influenced by TGD operation (corresponding to those in Fig. 6), while Fig. 7(b) presents those without TGD. By subtracting the daily interaction rates in Fig. 7(b) from those in Fig. 7(a), we obtain the differences in these rates between the scenarios with and without the TGD, as shown in Fig. 7(c).

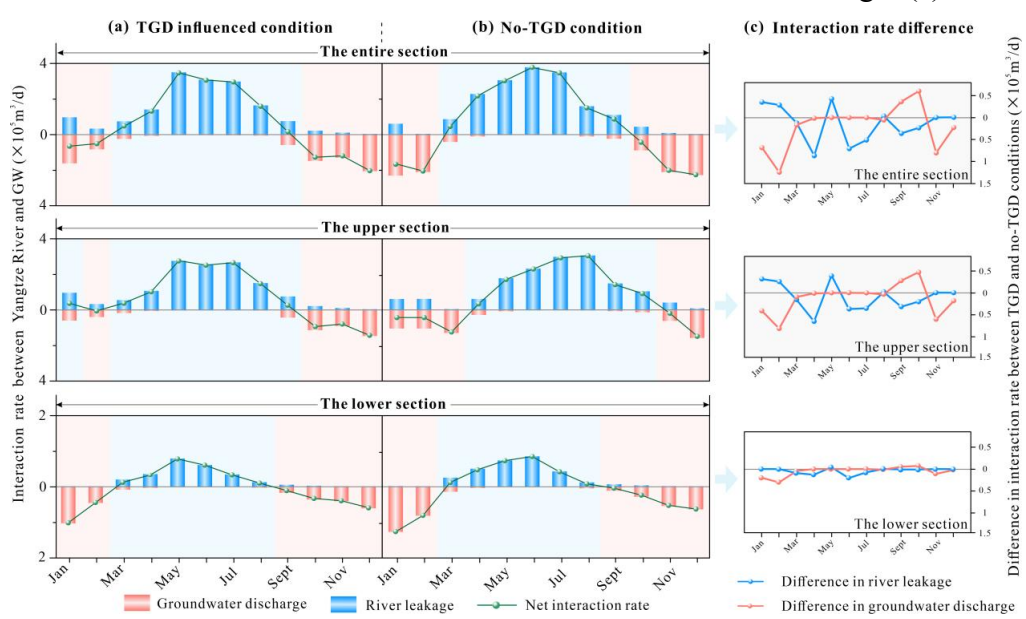


Figure 7: Temporal variations in the river leakage rates, groundwater discharge rates and net exchange rates under TGD-influenced (a) and no-TGD conditions (b) between the Yangtze River and groundwater. Fluxes are positive for river leakage to the aquifer and negative for groundwater discharge to the river. (c) Interaction rate difference between TGD and no-TGD conditions in river leakage and groundwater discharge. More detailed information can be found in Table A3.





443

444

445

446

447

448

449

450

451

452

453

454

455

456

457

458

459

460

461

462

463

464

465

466

467

Figure 7(b) shows that regardless of TGD operation, the Yangtze Rive leakage to groundwater dominates from March to September in both the upper and lower sections of the Four-Lake basin. In contrast, groundwater discharge to the Yangzte River prevails from October to February of the following year. Across the entire section of stream, the peak net exchange rate occurs in June, reaching 3.77×10⁵ m³/d. Spatially, the net flow direction (river leakage versus groundwater discharge) differs between the upper and lower sections. In the upper section, the rate of river leakage to groundwater consistently exceeds the discharge rate, regardless of TGD regulation. With a comparison between Figs. 7(a) and 7(b) by calculating the average net exchange rates for both flooding season (from June to September) and dry period (from November to April), one can find that TGD operations significantly suppress the natural river-groundwater exchange. Under TGD regulation, the net exchange rate across the entire section decreased by 19.3% and 41.8% during the flooding and dry periods, respectively, compared to natural conditions. This suppression was more pronounced in the upper section, where the net exchange dropped by 40.6% during the dry period, contrasting with a decrease of 23.8% in the lower section. In addition, it can be visually inferred from Fig. 7(c) that a considerable number of values lie below zero. This indicates that, compared to the natural conditions, TGD operations lead to a reduction in river leakage to groundwater for nine months of the year and a decrease in groundwater discharge to the river for ten months in the upper section. Notably, in the lower section, the fluxes in both directions (river leakage and groundwater discharge) are reduced throughout nearly the entire year. These findings demonstrate that the TGD attenuates flood peaks and elevates low flows, thereby reducing the seasonal amplitude of river stages and narrowing the river-aquifer hydraulic gradient. Consequently, the exchange dynamics become more balanced and stable. The upper section, being directly subject to regulatory releases,





468 exhibits a more pronounced response in net exchange, particularly during the dry 469 season. As also evident from the mapped zone of the Yangtze River's lateral influence 470 on groundwater in Fig. 3, the groundwater response to river stage changes is visibly 471 weaker in the lower section, particularly near Honghu Lake, compared to the upper 472 section. As shown by the net interaction curve for the upper section (Fig. 7), the 473 period from January to March, which was naturally characterized by groundwater 474 discharge to the river, transitions to a state of weak river leakage to the aquifer 475 following the TGD-induced rise in dry-season river stage. This flow reversal occurs 476 because the dry-season hydraulic gradient is inherently small; thus, even a modest 477 stage increase can induce a substantial relative change, making the regulatory influence more pronounced during dry months than in the flood season. 478

5 Conclusion

479

486

487

488

489

490

This study integrated large-scale monitoring data from multiple profiles along the Yangtze River in the Four-Lake Basin, on which a spatial response analysis of water levels was performed followed by a coupled surface water-groundwater modeling framework. Then, the interactions between the Yangtze River and groundwater were systematically investigated through both qualitative and quantitative analyses. The key findings are as follows:

(1) Spatial variability of the Yangtze River influence. The lateral influence zone of the Yangtze River on groundwater in the Four-Lake Basin has been quantified for the first time, revealing a band-like pattern with a high degree of spatial heterogeneity. The lateral influence range varies from 1.94 km (HH1 profile) to 12.77 km (ZJ profile) across the Four-Lake Basin.





- (2) Performance of the newly proposed model. Given the significant influence of rainfall and the surface water network on groundwater in the Four-Lake basin, the SWAT-MODFLOW model is capable of accurately quantifying the exchange fluxes between the Yangtze River and groundwater.
- (3) Spatial-temporal interaction dynamics between the Yangzte River and groundwater. Temporally, the Yangtze River leakage to groundwater is greater during the drawdown period than during the flooding period. Conversely, groundwater discharge to the Yangzte river is higher in the impounding period than in the dry period. This dynamic is dictated by the combined effects of seasonal TGD regulation and the local hydroclimate. Spatially, the interaction intensity between the Yangtze River and groundwater is markedly higher in the upper section of the Four-Lake Basin than the lower section, which is attributed to the integrated influences of the TGD, the thalweg configuration, and riparian hydrogeology.
- (4) The impacts of the TGD operation on the Yangtze River-groundwater interaction. By modulating river stages, TGD operations reduce temporal variability in Yangtze River-groundwater exchange rates, thereby promoting more balanced and stable dynamics. This effect is most direct and pronounced in the upper section during the dry period, whereas its influence attenuates downstream.





511 Appendix A

512 513

Table A1 Aquifer hydrogeologic parameters for MODFLOW model.

| Parameter Zone | Horizontal Conductivity $K_{xy} \text{ (m/d)}$ | | Vertical Con | nductivity | Specific Yield | Specific Storage |
|-------------------|--|----------|--------------|------------|-------------------|---------------------|
| | | | K_z (m/d) | | $S_{\mathcal{Y}}$ | S_s (L-1) |
| | Unconfined | Confined | Unconfined | Confined | Unconfined | Confined |
| | Aquifer | Aquifer | Aquifer | Aquifer | Aquifer | Aquifer |
| 1 | 1.00 | 9.75 | 0.150 | 1.1 | | 0.0004 |
| 2 | 1.5 | 16 | 0.302 | 1.6 | 0.021 | 0.0022 |
| 3 | 0.79 | 7.7 | 0.120 | 0.85 | 0.021 | 0.001 |
| 4 | 0.54 | 4.9 | 0.081 | 0.57 | | 0.0023 |

514515

516

Table A2 SWAT model calibrated parameters with adjusted values and sensitivity ranking.

| Symbol | scale | Calibrated Value | <i>t</i> -value | <i>p</i> -value | Sensibility |
|------------|-----------|------------------|-----------------|-----------------|-------------|
| GWQMN | 0-5000 | 186.90 | -30.89 | 0.00 | 1 |
| REVAPMN | 0-500 | 188.31 | 15.60 | 0.00 | 2 |
| GW_DELAY | 0-500 | 232.39 | -1.97 | 0.05 | 3 |
| CH_N2 | -0.01-0.3 | 0.11 | 1.91 | 0.06 | 4 |
| SOL_BD | 0.9-2.5 | 1.13 | 1.79 | 0.07 | 5 |
| CH_N1 | 0.01-30 | 20.30 | -1.48 | 0.14 | 6 |
| CH_K2 | -0.01-500 | 27.39 | -1.22 | 0.22 | 7 |
| SURLAG | 0.05-24 | 15.11 | -1.21 | 0.23 | 8 |
| GW_REVAP | 0.02-0.2 | 0.17 | -1.20 | 0.23 | 9 |
| SOL_AWC | 0-1 | 0.00 | 0.90 | 0.37 | 10 |
| ESCO | 0.01-1 | 0.36 | 0.88 | 0.38 | 11 |
| OV_N | 0.01-30 | 17.89 | -0.81 | 0.42 | 12 |
| ALPHA_BNK | 0-1 | 0.33 | -0.79 | 0.43 | 13 |
| ALPHA_BF | 0-1 | 0.22 | -0.47 | 0.64 | 14 |
| SOL_K | 0-2000 | 1766.62 | 0.38 | 0.70 | 15 |
| EPCO | 0.01-1 | 0.38 | 0.16 | 0.87 | 16 |
| CN2 | 35-98 | 35.34 | -0.01 | 0.99 | 17 |





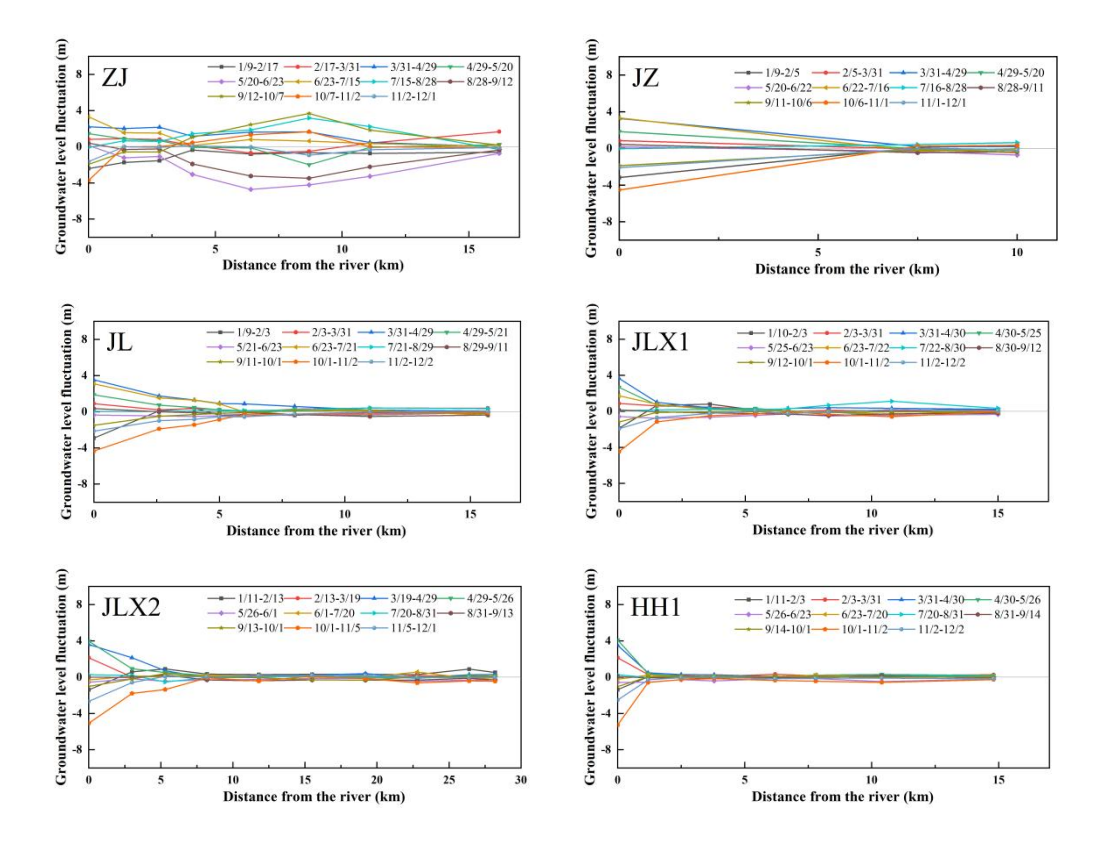
Table A3 Average river leakage, groundwater discharge, and net exchange rates (average of 2011 to 2013) under TGD regulated operation and natural conditions between the Yangtze River and groundwater for the entire section, upper section, and lower section.

| | TGD reg | gulated operati | ion (m³/d) | Natural condition (m ³ /d) | | | |
|-----------|---------------------------------|---------------------------------|----------------------------|---------------------------------------|------------------------------------|----------------------------|--|
| Month | GW to SW interaction rate | SW to GW interaction rate | Net interaction rate | GW to SW interaction rate | SW to GW interaction rate | Net interaction rate | |
| | | Т | he entire secti | on | | | |
| January | 160398.61 | 95125.29 | -65273.32 | 228615.16 | 60134.45 | -168480.71 | |
| February | 82495.96 | 31721.82 | -50774.14 | 207866.07 | 3207.19 | -204658.88 | |
| March | 23711.71 | 72382.68 | 48670.97 | 39499.77 | 85539.23 | 46039.45 | |
| April | 6623.12 | 138788.77 | 132165.65 | 8323.54 | 226616.07 | 218292.53 | |
| May | 243.95 | 346652.48 | 346408.53 | 392.89 | 303461.94 | 303069.04 | |
| June | 164.13 | 306211.00 | 306046.87 | 177.75 | 376947.00 | 376769.25 | |
| July | 820.53 | 296601.61 | 295781.08 | 738.01 | 347322.58 | 346584.57 | |
| August | 3511.69 | 161664.84 | 158153.15 | 8772.14 | 158542.26 | 149770.11 | |
| September | 57918.17 | 73367.00 | 15448.83 | 21667.64 | 109546.30 | 87878.66 | |
| October | 147234.71 | 19725.15 | -127509.56 | 86604.52 | 43101.06 | -43503.45 | |
| November | 128486.87 | 8695.77 | -119791.10 | 208785.13 | 8053.23 | -200731.90 | |
| December | 204551.52 | 1709.64 | -202841.88 | 227181.03 | 1014.45 | -226166.58 | |
| | | Т | he upper secti | on | | | |
| January | 58348.03 | 95037.48 | 36689.45 | 102956.55 | 60063.03 | -42893.52 | |
| February | 38014.14 | 31633.79 | -6380.36 | 127649.18 | 3134.64 | -124514.54 | |
| March | 16301.00 | 53726.03 | 37425.03 | 26561.48 | 60730.62 | 34169.13 | |
| April | 4151.07 | 106185.73 | 102034.66 | 5809.77 | 176407.07 | 170597.30 | |
| May | 119.41 | 273851.55 | 273732.14 | 193.20 | 229956.61 | 229763.42 | |
| June | 0.00 | 251251.33 | 251251.33 | 43.90 | 291955.00 | 291911.10 | |
| July | 189.88 | 265419.35 | 265229.48 | 195.26 | 304419.35 | 304224.09 | |
| August | 1747.66 | 149041.61 | 147293.95 | 5534.11 | 146825.81 | 141291.70 | |
| September | 41711.41 | 67952.03 | 26240.62 | 11612.61 | 103078.03 | 91465.43 | |
| October | 112226.70 | 17772.32 | -94454.38 | 59672.18 | 39762.87 | -19909.31 | |
| November | 88397.23 | 8008.71 | -80388.52 | 155803.43 | 7426.35 | -148377.08 | |
| December | 144907.90 | 1609.14 | -143298.76 | 164598.90 | 935.00 | -163663.90 | |
| | | 1 | The lower section | on | | | |
| January | 102049.81 | 88.41 | -101961.40 | 125658.55 | 71.12 | -125587.42 | |
| February | 44481.75 | 88.01 | -44393.74 | 80217.18 | 72.57 | -80144.61 | |





| March | 7410.79 | 19464.46 | 12053.67 | 12938.26 | 24809.01 | 11870.76 |
|-----------|----------|----------|-----------|----------|----------|-----------|
| April | 2472.04 | 34925.19 | 32453.15 | 2513.73 | 50209.80 | 47696.07 |
| May | 124.54 | 78462.61 | 78338.07 | 199.69 | 73506.32 | 73306.63 |
| June | 164.13 | 60520.87 | 60356.74 | 133.85 | 84992.97 | 84859.12 |
| July | 630.65 | 34033.13 | 33402.48 | 542.75 | 42902.87 | 42360.12 |
| August | 1764.04 | 12076.83 | 10312.79 | 3238.03 | 11716.11 | 8478.07 |
| September | 16207.16 | 4955.09 | -11252.07 | 10055.03 | 6469.54 | -3585.49 |
| October | 35008.08 | 1889.88 | -33118.21 | 26932.46 | 3337.93 | -23594.54 |
| November | 40089.60 | 684.73 | -39404.87 | 52981.83 | 626.87 | -52354.95 |
| December | 59643.16 | 100.48 | -59542.68 | 62582.29 | 79.45 | -62502.84 |







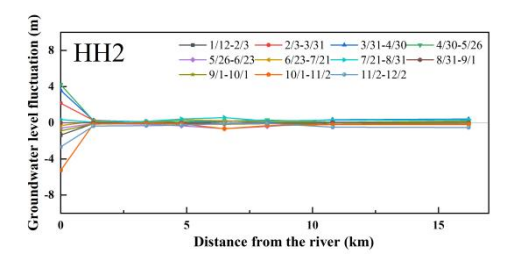


Figure A1. Groundwater level fluctuation *y* versus distance from the river *x* for each monitoring profile.

In the legend, the A and B in "A/B" represent month and data, respectively

526

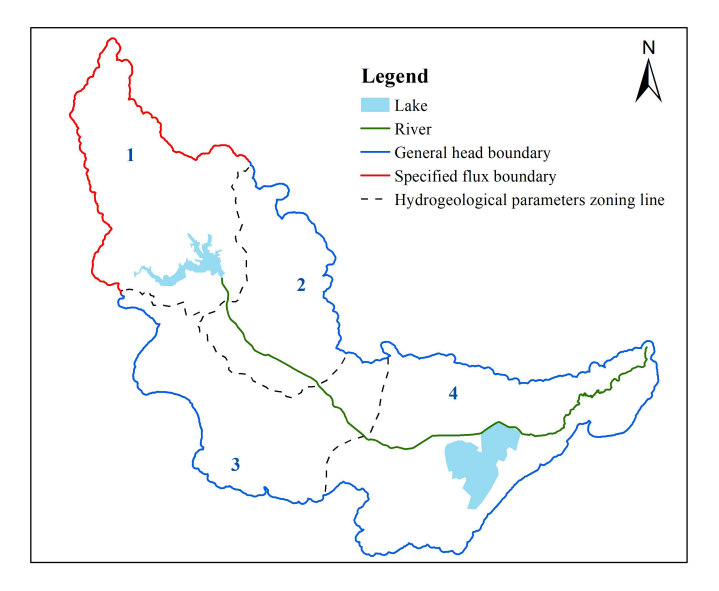
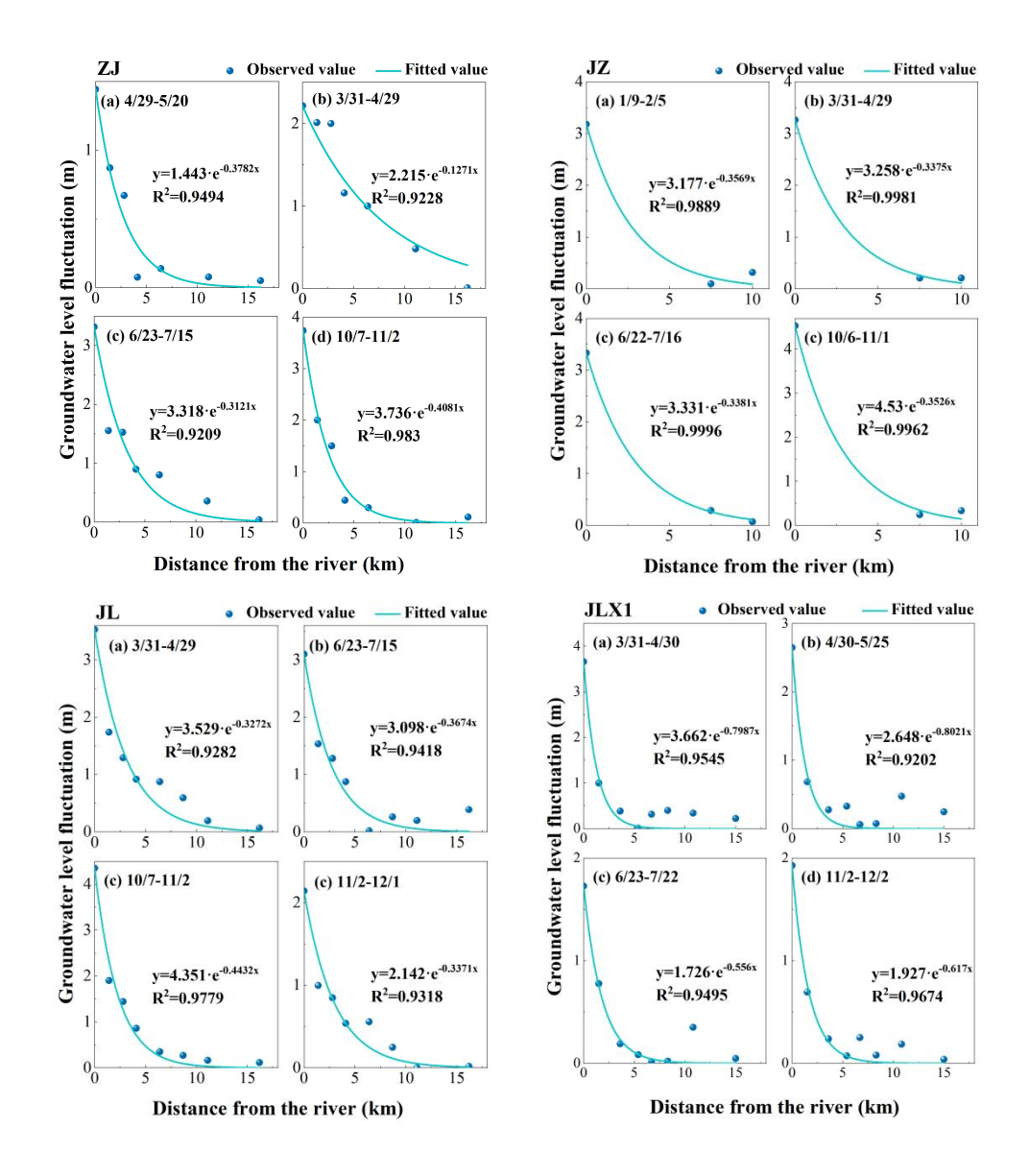


Figure A2. Groundwater model boundary and hydrogeologic parameter zones.











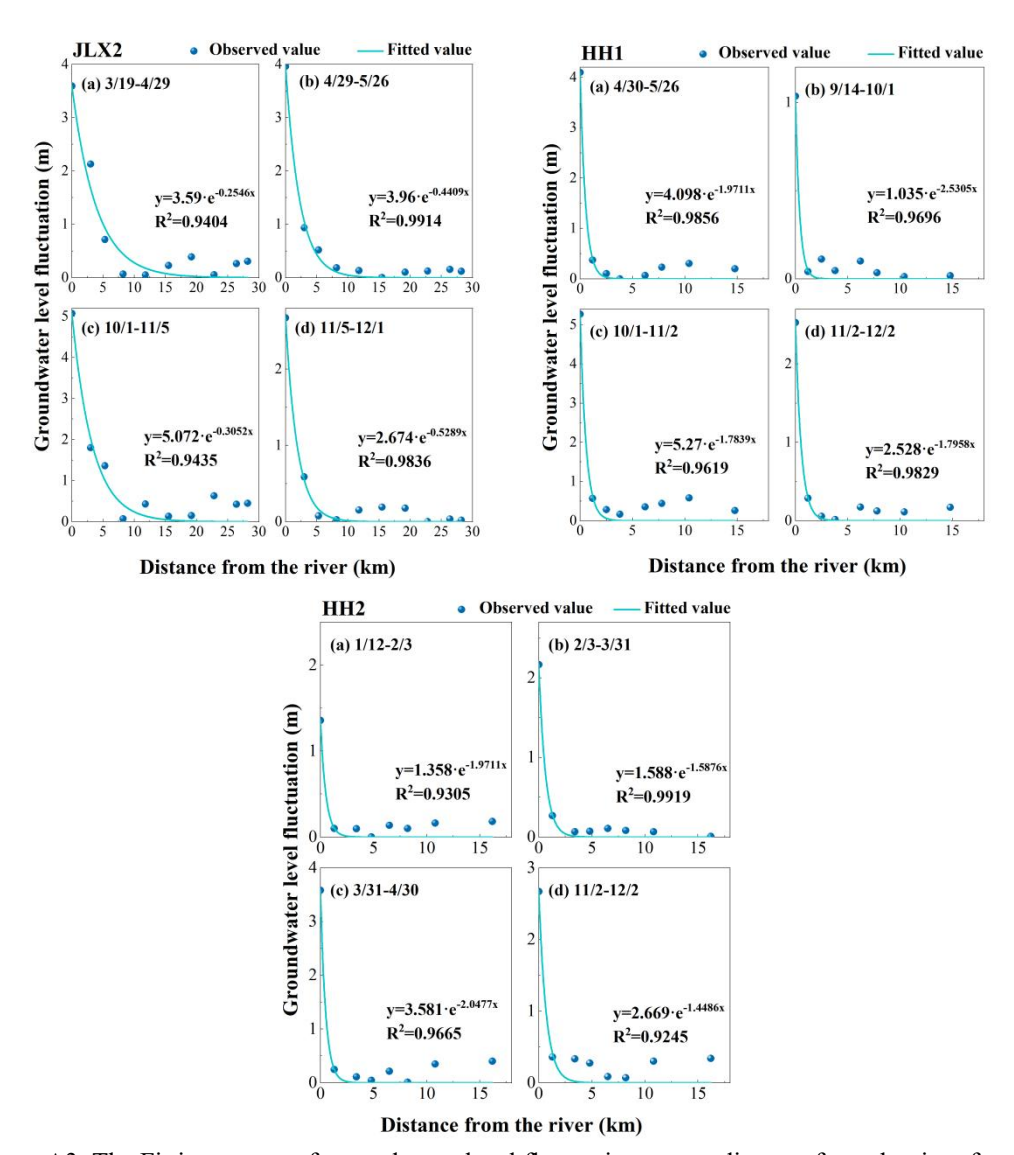


Figure A3. The Fitting curves of groundwater level fluctuation versus distance from the river for each monitoring profile.





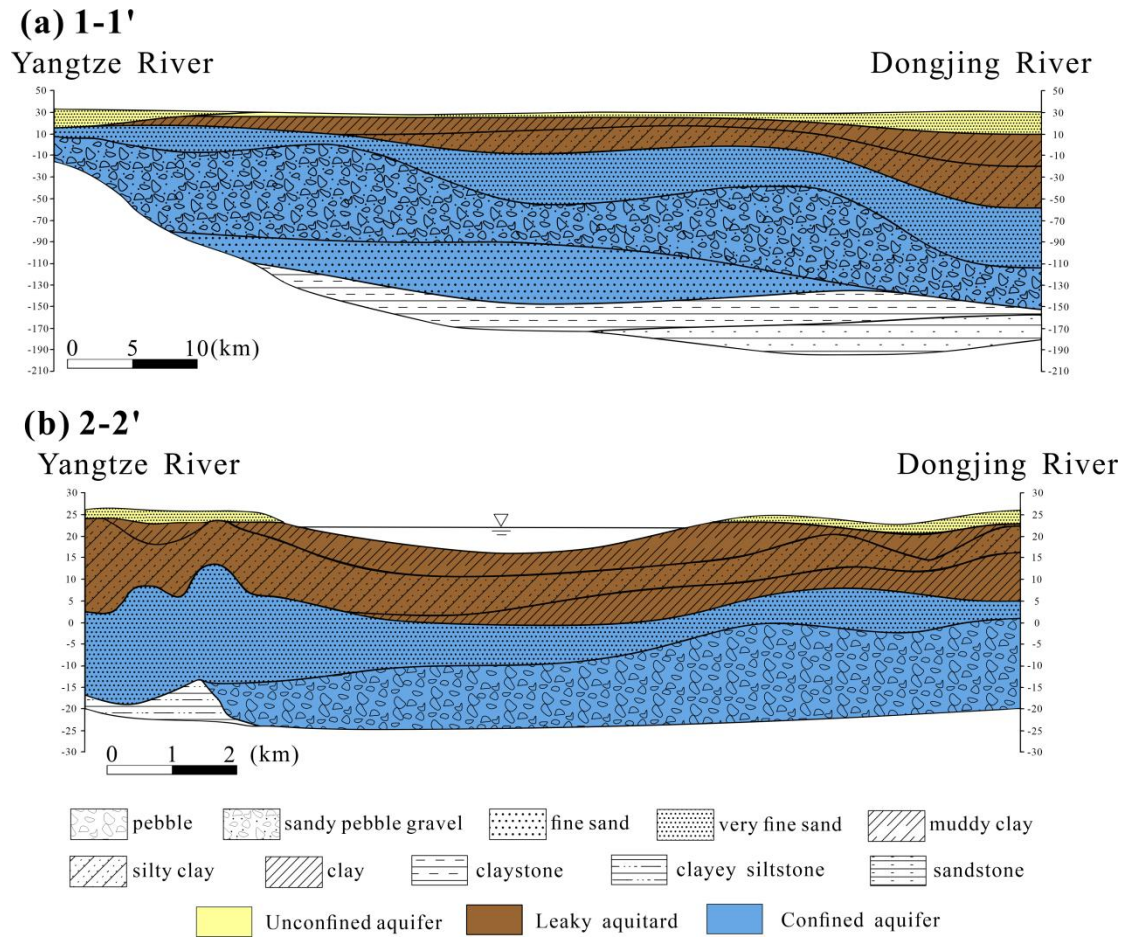


Figure A4. (a) Stratigraphic profile 1-1' near Jiangling (JL) Profile ; (b) Stratigraphic profile 2-2' near Honghu (HH) Profile.



536

537

538

539



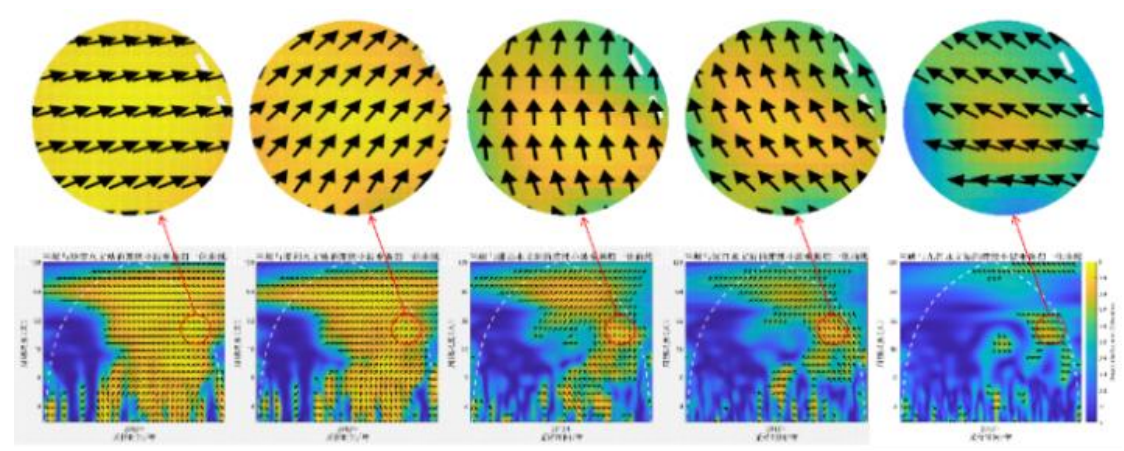


Figure A5. Wavelet correlation between the Three Gorges Reservoir water level and the water levels at Shashi, Jianli, Luoshan, Hankou, and Jiujiang hydrological stations on the Yangtze River in 2012.

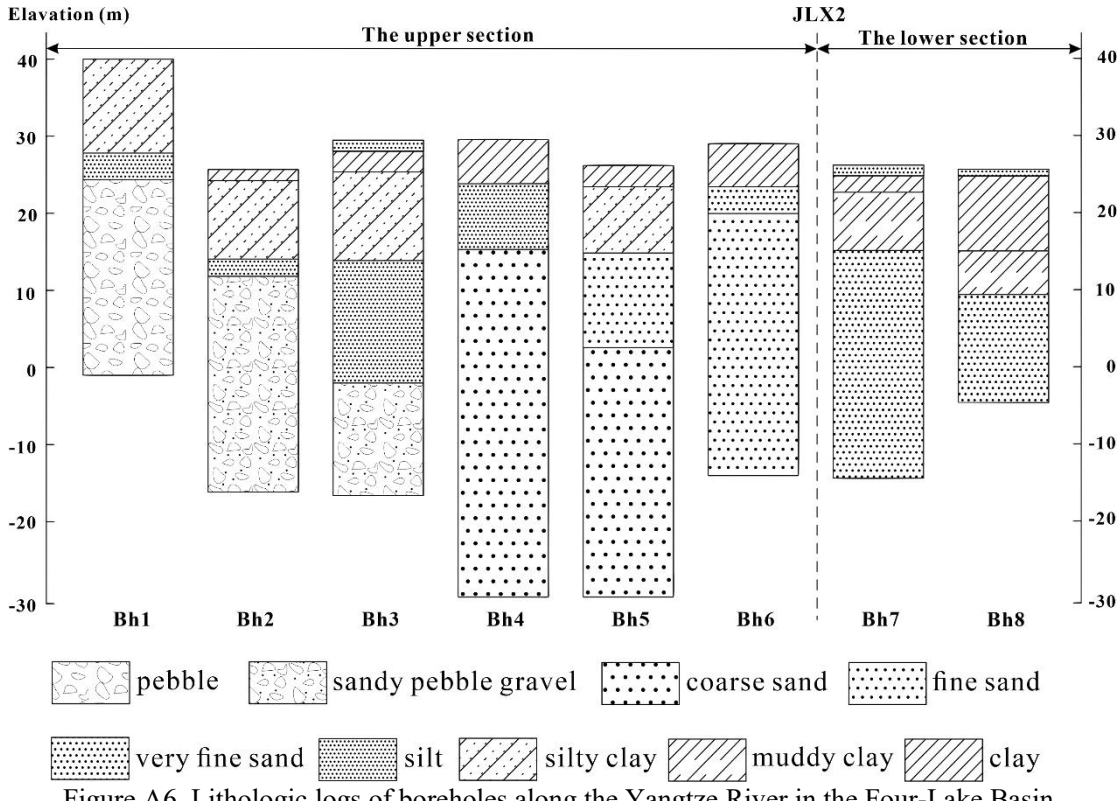


Figure A6. Lithologic logs of boreholes along the Yangtze River in the Four-Lake Basin.





542 Code and data availability

- Additional information regarding methodology and results is provided in the
- 544 Supplement.

545 Author contributions

- Qi Zhu: conceptualization, formal analysis and writting; Ye Kang: methodology,
- 547 investigation and drawing; Zhang Wen: project administration and software; Hui Liu:
- 548 Funding acquisition and idea; Luguang Liu: monitoring work; Yan Li: field data
- 549 collection; Xu Li: model support, Eungyu Park: supervision and validation.

550 Competing interests

The authors declare that they have no conflict of interest.

552 Financial support

- This research was partially supported by the National Natural Science
- 554 Foundation of China (Grant Numbers: U2340206; U23A2042; 42572313; 42272290)
- 555 the Natural Science Foundation of Hubei Province (2023AFD194), and the Hubei
- 556 Province Science and Technology Innovation Platform Project (Grant Number
- 557 2025CSA007).

558 References

- 559 Aliyari, F., Bailey, R. T., Tasdighi, A., Dozier, A., Arabi, M., Zeiler, K.: Coupled
- 560 SWAT-MODFLOW model for large-scale mixed agro-urban river basins,





- 561 Environ. Modell. Softw., 115, 200–210, doi: 10.1016/j.envsoft.2019.02.014,
- 562 2019.
- Deng, K., Yang, S., Lian, E., Li, C., Yang, C., Wei, H.: Three Gorges Dam alters the
- Changiang (Yangtze) river water cycle in the dry seasons: Evidence from H-O
- isotopes, Sci. Total Environ., 562, 89–97, doi: 10.1016/j.scitotenv.2016.03.213,
- 566 2016.
- 567 Dewey, C., Fox, P. M., Bouskill, N. J., Dwivedi, D., Nico, P., Fendorf S.: Beaver
- dams overshadow climate extremes in controlling riparian hydrology and water
- quality. Nat. Commun., 13, 6509, doi: 10.1038/s41467-022-34022-0, 2022.
- 570 Du, Y., Ma, T., Deng, Y., Shen, S., Lu, Z.: Characterizing groundwater/surface-water
- interactions in the interior of Jianghan Plain, central China, Hydrogeol. J., 26(4),
- 572 1047–1059, doi: 10.1007/s10040-017-1709-7, 2018.
- 573 Esri.: World Ocean Base [Data set]. ArcGIS Online. Retrievedfrom
- 574 https://services.arcgisonline.com/ArcGIS/rest/services/Ocean/World Ocean Bas
- 575 e/MapServer, 2023.
- 576 Gao, Y., Zhang, W., Li, Y., Wu, H., Yang, N., Hui, C.: Dams shift microbial
- 577 community assembly and imprint nitrogen transformation along the Yangtze
- 578 River, Water Res., 189, 116579, doi:10.1016/j.watres.2020.116579, 2021.
- 579 Guo, W., Zhou, H., Jiao, X., Huang, L., Wang, H.: Evaluation of hydrological regime
- alteration and ecological effects in the middle and lower of the Yangtze River,
- 581 China, Water Supply, 22(6), 5957-5973., doi: 10.2166/ws.2022.229, 2022.
- 582 He B., Cai S.: The Three-Gorge Project and dynamics of shallow confined water in
- the area of the middle reaches of the Yangtze River. Resources and Environment
- in the Yangtze Basin, 8(1), doi: CNKI:SUN:CJLY.0.1999-01-014, 1999.
- Hu, M., Yao, M., Wang, Y., Pan, Z., Wu, K., Jiao, X., Chen, D.: Influence of nitrogen
- inputs, dam construction and landscape patterns on riverine nitrogen exports in





- the Yangtze River basin during 1980–2015, J. Hydrol., 617, 129109, doi:
- 588 10.1016/j.jhydrol.2023.129109, 2023.
- Hu, M., Zhou, P., Chen, C.: Study on coupling of typical elements in surface water
- and groundwater in the middle reaches of the Yangtze River, China, J. Hydrol.,
- 591 626, 130298, doi: 10.1016/j.jhydrol.2023.130298, 2023.
- Huang, P., Zhou, A., Ma, C., Guo, J., Wang, Y., Fan, W., Li, W.: Impact of the Three
- Gorges Dam on the spatial and temporal variation of groundwater level in
- Jianghan Plain using STL algorithm, Environ. Earth Sci., 82(18), 417, doi:
- 595 10.1007/s12665-023-11110-y, 2023.
- 596 Huang, S., Xia, J., Zeng, S. Wang, Y., She, D.: Effect of Three Gorges Dam on
- Poyang Lake water level at daily scale based on machine learning, Journal of
- 598 Geographical Sciences, 31, 1598-1614, doi: 10.1007/s11442-021-1913-1, 2021.
- 599 Jiang, X., Ma, R., Ma, T., Sun, Z.: Modeling the effects of water diversion projects on
- surface water and groundwater interactions in the central Yangtze River basin,
- 601 Sci. Total Environ., 830, 154606, doi: 10.1016/j.scitotenv.2022.154606, 2022.
- 602 Lai, X., Zou, H., Jiang, J., Jia, J., Liu, Y., Wei, W.: Hydrological dynamics of the
- Yangtze River-Dongting lake system after the construction of the three Gorges
- dam, Scientific Reports, 15(1), 50, doi: 10.1038/s41598-024-83751-3, 2025.
- 605 Liu, Y., Wang, H., Wu, Y., Zhao, Y., Ren, X.: Aquifer response to stream-stage
- fluctuations: field tests and analytical solution for a case study of the Yangtze
- 607 River in Wuhan, China, Water, 13(17), 2388, doi: 10.3390/w13172388, 2021.
- 608 Maavara, T., Chen, Q., Van Meter, K., Brown, L. E., Zhang, J., Ni, J., Zarfl, C.: River
- dam impacts on biogeochemical cycling. Nat. Rev. Earth Env., 1(2), 103-116,
- doi:10.1038/s43017-019-0019-0, 2020





- Palmer, M., Ruhi, A.: Linkages between flow regime, biota, and ecosystem processes:
- Implications for river restoration, Science, 365, 1264, doi:
- 613 10.1126/science.aaw2087, 2019,
- 614 Poff, N. L., Allan, J. D., Bain, M. B., Karr, J. R., Prestegaard, K. L, Richter, B. D.,
- Sparks, R. E., Stromberg, J. C.: The natural flow regime, Bioscience, 47(11),
- 616 769-784, doi: 10.2307/1313099, 1997.
- 617 Song, X., Chen, X., Zachara, J. M., Gomez-velez, J. D., Shuai, P., Ren, H., Hammond,
- 618 G. E.: dynamics control transit time distributions and biogeochemical reactions
- in a dam-regulated river corridor, Water Resour. Res., 56(9), e2019WR026470,
- doi: 10.1029/2019WR026470.
- 621 Sun, Z., Huang, Q., Opp, C., Hennig, T., Marold, U.: Impacts and implications of
- major changes caused by the Three Gorges Dam in the middle reaches of the
- Yangtze River, China, Water Resour. Manag., 26, 3367-3378, doi:
- 624 10.1007/s11269-012-0076-3, 2012.
- 625 Van Cappellen, P., Maavara, T.: Rivers in the Anthropocene: Global scale
- 626 modifications of riverine nutrient fluxes by damming, Ecohydrol. Hydrobiol.,
- 627 16(2), 106-111, doi: 10.1016/j.ecohyd.2016.04.001, 2016.
- 628 Wang, J., Sheng, Y., Gleason, C.J., Wada, Y.: Downstream Yangtze River levels
- impacted by Three Gorges Dam, Environ. Res. Lett., 8(4), 044012, doi:
- 630 10.1088/1748-9326/8/4/044012, 2013.
- Wang, J., Wörman, A.: Spectral analysis of river resistance and aquifer diffusivity in
- a river-confined aquifer system. Water Resour. Res., 55(10), 8046–8060, doi:
- 633 10.1029/2018WR024639, 2019.
- 634 Wang, X., Cai, X., Yang, C., Lv, X., Li, E., Wang, Z.: Evolution and ecological
- restoration of riverine and lacustrine wetland system in the middle reaches of the





- Yangtze River. Bulletin of National Natural Science Foundation of China, 36,(3)
- 637 398–405, doi: 10.16262/j.cnki.1000-8217.2022.03.006, 2022.
- Wang, Y., Rhoads, B. L., Wang, D., Assessment of the flow regime alterations in the
- middle reach of the Yangtze River associated with dam construction: potential
- ecological implications, Hydrol. Processes, 30(21), 3949-3966, doi:
- 641 10.1002/hyp.10921, 2016.
- 642 Wen, Z., Zhan, H., Wang, Q., Liang, X., Ma, T., Chen, C.: Well hydraulics in
- pumping tests with exponentially decayed rates of abstraction in confined
- aguifers, J. Hydrol., 548, 40-45, doi: 10.1016/j.jhydrol.2017.02.046, 2017.
- 645 World Bank, 2023. Yangtze River Protection and Ecological Restoration Program
- Program for Results (Hubei).
- 647 Wu, X., Wang, L., Cao, Q., Niu, Z., Dai, X.: Regional climate change and possible
- causes over the Three Gorges Reservoir Area, Sci. Total Environ., 903, 166263,
- doi: 10.1016/j.scitotenv.2023.166263, 2023.
- 650 Xie, Y., Tang, Y., Chen, X., Li, F., Deng, Z.: The impact of Three Gorges Dam on the
- downstream eco-hydrological environment and vegetation distribution of East
- 652 Dongting Lake, Ecohydrology, 8(4), 738-746, doi: 10.1002/eco.1543, 2014.
- 653 Xiong, J., Yin, J., Kyaw Tha Paw U, Zhao, S., Qiu, G., Liu, Z.: How the three Gorges
- Dam affects the hydrological cycle in the mid-lower Yangtze River: a
- perspective based on decadal water temperature changes, Environ. Res. Lett., 15,
- 656 014002, doi: 10.1088/1748-9326/ab5d9a, 2020.
- 657 Yang, Y., Yuan, Y., Xiong, G., Yin, Z., Guo, Y., Song, J., Zhu, X., Wu, J., Wang, J.,
- Wu, J.: Patterns of nitrate load variability under surface water-groundwater
- interactions in agriculturally intensive valley watersheds, Water Res., 267,
- 660 122474, doi: 10.1016/j.watres.2024.122474, 2024.





- 661 Yang, S., Milliman, J. D., Xu, K., Deng, B., Zhang, X., Luo, X.: Downstream
- sedimentary and geomorphic impacts of the Three Gorges Dam on the Yangtze
- River, Earth-Sci. Rev., 138, 469-486, doi: 10.1016/j.earscirev.2014.07.006, 2014.
- 664 Yang, S., Zhang, J., Xu, X.: Influence of the Three Gorges Dam on downstream
- delivery of sediment and its environmental implications, Yangtze River,
- Geophys. Res. Lett., 34(10), doi: 10.1029/2007GL029472, 2007.
- Zhang, Q., Li, L., Wang, Y., Werner, A., Xin, P., Jiang, T., Barry, D.: Has the Three-
- Gorges Dam made the Poyang Lake wetlands wetter and drier? Geophys. Res.
- Lett., 39(20), 28, doi: 10.1029/2012GL053431, 2012.
- 670 Zhang, S., Zhai, X., Yang, P., Xia, J., Hu, S., Zhou, L., Fu, C.: Ecological health
- analysis of wetlands in the middle reaches of Yangtze River under changing
- 672 environment, Int. J. Digit. Earth, 16(1), 3125–3144, doi:
- 673 10.1080/17538947.2023.2244471, 2023.
- 674 Zhou, M., Xia, J., Deng, S., Shen, J., Mao, Y.: Modelling of phosphorus and
- 675 nonuniform sediment transport in the Middle Yangtze River with the effects of
- channel erosion, tributary confluence and anthropogenic emission. Water Res.,
- 677 243, 120304, doi: 10.1016/j.watres.2023.120304. 2023.
- 678 Zhou, Y., Wang, Y., Li, Y., Zwahlen, F., Boillat, J.: Hydrogeochemical characteristics
- of central Jianghan Plain, China. Environ. Earth Sci., 68(3), 765–778, doi:
- 680 10.1007/s12665-012-1778-9, 2013.